nature medicine

Slit2 signaling through Robo1 and Robo2 is required for retinal neovascularization

Nicolas Rama[1–3,8], Alexandre Dubrac[4,8], Thomas Mathivet[5], Róisín-Ana Ní Chárthaigh[1–3], Gael Genet[4], Brunella Cristofaro[5], Laurence Pibouin-Fragner[5], Le Ma[6], Anne Eichmann[4,5,7] & Alain Chédotal[1–3]

Ocular neovascular diseases are a leading cause of blindness. Vascular endothelial growth factor (VEGF) blockade improves vision, but not all individuals respond to anti-VEGF treatment, making additional means to prevent neovascularization necessary. Slit-family proteins (Slits) are ligands of Roundabout (Robo) receptors that repel developing axons in the nervous system. Robo1 expression is altered in ocular neovascular diseases, and previous *in vitro* studies have reported both pro- and anti-angiogenic effects of Slits. However, genetic evidence supporting a role for Slits in ocular neovascularization is lacking. Here we generated conditional knockout mice deficient in various Slit and Robo proteins and found that Slit2 potently and selectively promoted angiogenesis via Robo1 and Robo2 in mouse postnatal retina and in a model of ocular neovascular disease. Mechanistically, Slit2 acting through Robo1 and Robo2 promoted the migration of endothelial cells. These receptors are required for both Slit2- and VEGF-induced Rac1 activation and lamellipodia formation. Thus, Slit2 blockade could potentially be used therapeutically to inhibit angiogenesis in individuals with ocular neovascular disease.

Ocular neovascular diseases are the most common cause of vision loss, affecting millions of people in the industrialized world. Such diseases include the wet form of age-related macular degeneration (AMD), diabetic retinopathy (DR), retinopathy of prematurity (the main cause of blindness in young children) and corneal inflammation. Each of these diseases is characterized by excessive angiogenesis accompanied by breakdown of the endothelial barrier and vascular leakage, leading to edema, hemorrhage and retinal detachment, which compromise vision. Treatment of excessive angiogenesis has relied on the inhibition of a single factor, VEGF, with some therapeutic success[1–3]. However, factors other than VEGF contribute to angiogenesis, and the identification of alternative pathways to block excessive angiogenesis and vascular leakage is of enormous therapeutic interest.

Slit ligands, secreted chemorepellents of growing axons and migrating neurons, signal through receptors of the Robo family[4–6]. Slits also are involved in the development of many organs and have been implicated in cancer. Three Slit ligands (Slit1–3) and four Robo receptors (Robo1–4) have been characterized in mammals on the basis of structural similarities. Although it was once thought that all Robo receptors bind Slits, mammalian Robo3 and Robo4 lack the key amino acid residues required for Slit binding[7,8]. Slit2 and Slit3 can inhibit VEGF-induced endothelial cell migration and permeability *in vitro* and vascular leakage in mice[9–12], suggesting that Slits could be used to alleviate edema in individuals with DR and AMD. However, other studies have shown pro-angiogenic functions of Slits[13–16]. These conflicting reports prompted us to investigate Slit actions in the eye using a genetic loss-of-function approach in mice. Although previous studies suggest that Robo4, an endothelial-cell-specific receptor, mediates Slit function, the lack of Slit binding to Robo4 has challenged this model[7]. Robo1 and, to a lesser extent, Robo2 are expressed by endothelial cells, but *in vivo* evidence supporting a role for Robo1 or Robo2 in the retinal vasculature is lacking, because the neonatal lethality observed in global *Slit2*- and *Robo2*-knockout animals precludes analysis of retinal vascular development, which occurs after birth. Here we generated mouse lines deficient in Slit1 and/or Slit2 or deficient in Robo1 and/or Robo2, and we used these mice to obtain genetic and biochemical evidence for a potent pro-angiogenic activity of Slit2 mediated by Robo1 and Robo2.

RESULTS

Slit2 is essential for retinal angiogenesis

We first defined the expression of all three *Slit* genes in the retina by *in situ* hybridization (**Fig. 1a**,**b** and **Supplementary Fig. 1a–c**). *Slit1* was expressed in horizontal cells in the inner nuclear layer (INL; **Fig. 1a** and **Supplementary Fig. 1b**) from postnatal day 5 (P5) onward. We also detected *Slit2* mRNA in the INL, in most bipolar neurons and possibly in some amacrine cells (**Fig. 1b** and **Supplementary Fig. 1a–c**). Slit1-expressing cells were located at a distance from blood vessels, but, as observed in heterozygous *Slit2*-knockout mice in which GFP was inserted in the *Slit2* locus[17], processes of

[1]INSERM UMR S968, Institut de la Vision, Paris, France. [2]Université Pierre et Marie Curie, Sorbonne Universités, Paris, France. [3]UMR 7210, CNRS, Paris, France. [4]Section of Cardiovascular Medicine, Department of Internal Medicine, Yale Cardiovascular Research Center, Yale University School of Medicine, New Haven, Connecticut, USA. [5]Center for Interdisciplinary Research in Biology (CIRB), Collège de France, Paris, France. [6]Department of Neuroscience, Farber Institute for Neurosciences, Thomas Jefferson University, Philadelphia, Pennsylvania, USA. [7]Department of Cellular and Molecular Physiology, Yale University School of Medicine, New Haven, Connecticut, USA. [8]These authors contributed equally to this work. Correspondence should be addressed to A.C. (alain.chedotal@inserm.fr) or A.E. (anne.eichmann@yale.edu).

Received 2 December 2014; accepted 25 March 2015; published online 20 April 2015; doi:10.1038/nm.3849

Slit2-expressing bipolar neurons extended underneath the vasculature (**Fig. 1c**), suggesting that Slit2 could target blood vessels. No *Slit1* or *Slit2* expression gradients were observed ahead of the vascular front (**Fig. 1a**,**b** and **Supplementary Fig. 1a**). We detected *Slit3* mRNA in the lens epithelium but not in the retina (**Supplementary Fig. 1a–c** and data not shown).

We next determined whether Slits could bind to retinal vessels by incubating whole-mount P5 retinas with Slit–alkaline phosphatase (Slit-AP) fusion proteins[18]. We used either full-length Slit2 (Slit2-AP) tagged at its N terminus, the region of Slit2 that binds Robo, or the second leucine-rich repeat domain of Slit1, Slit2 or Slit3 (Slit-D2-AP), which mediates Slit binding to Robo[19]. All Slit-AP probes strongly and selectively bound to the vasculature, in a pattern similar to that of VEGF-AP, which binds VEGF receptors on endothelial cells (**Fig. 1d**, **Supplementary Fig. 1d** and **Supplementary Table 1**), suggesting that Slit receptors are preferentially expressed in blood vessels in the postnatal retina.

To test Slit function in retinal angiogenesis, we generated a *Slit2*–conditional knockout allele (*Slit2*$^{lox/lox}$; **Supplementary Fig. 2**). *Slit2*$^{lox/lox}$ mice were crossed to mice expressing a tamoxifen-inducible Cre recombinase driven by the broadly expressed CAG promoter, generating CAG:*Slit2*$^{lox/lox}$ mice[20]. We also crossed these mice with *Slit1*-knockout mice (*Slit1*$^{-/-}$)[17] to inactivate both retina-expressed Slits. We injected tamoxifen into mice at birth (P0) and analyzed retinas at P7. We confirmed *Slit2* deletion in the retinas of tamoxifen-injected mice by *in situ* hybridization with a *Slit2* exon 8–specific riboprobe and by western blot using a Slit2-specific antibody (**Fig. 1e**,**f** and **Supplementary Fig. 2b**,**c**,**e**). At P7, the development of the retinal vasculature (number of branch points, retinal coverage and vascular progression) was comparable among wild-type, *Slit1*$^{+/-}$ and *Slit1*$^{-/-}$ mice (**Fig. 1g** and **Supplementary Figs. 2f** and **3a–c**). By contrast, the retinas of CAG:*Slit2*$^{lox/lox}$ mice exhibited severely reduced vessel branching and outgrowth; no significant additive effect was observed in double-mutant CAG:*Slit2*$^{lox/lox}$*Slit1*$^{-/-}$ mice (**Fig. 1g**

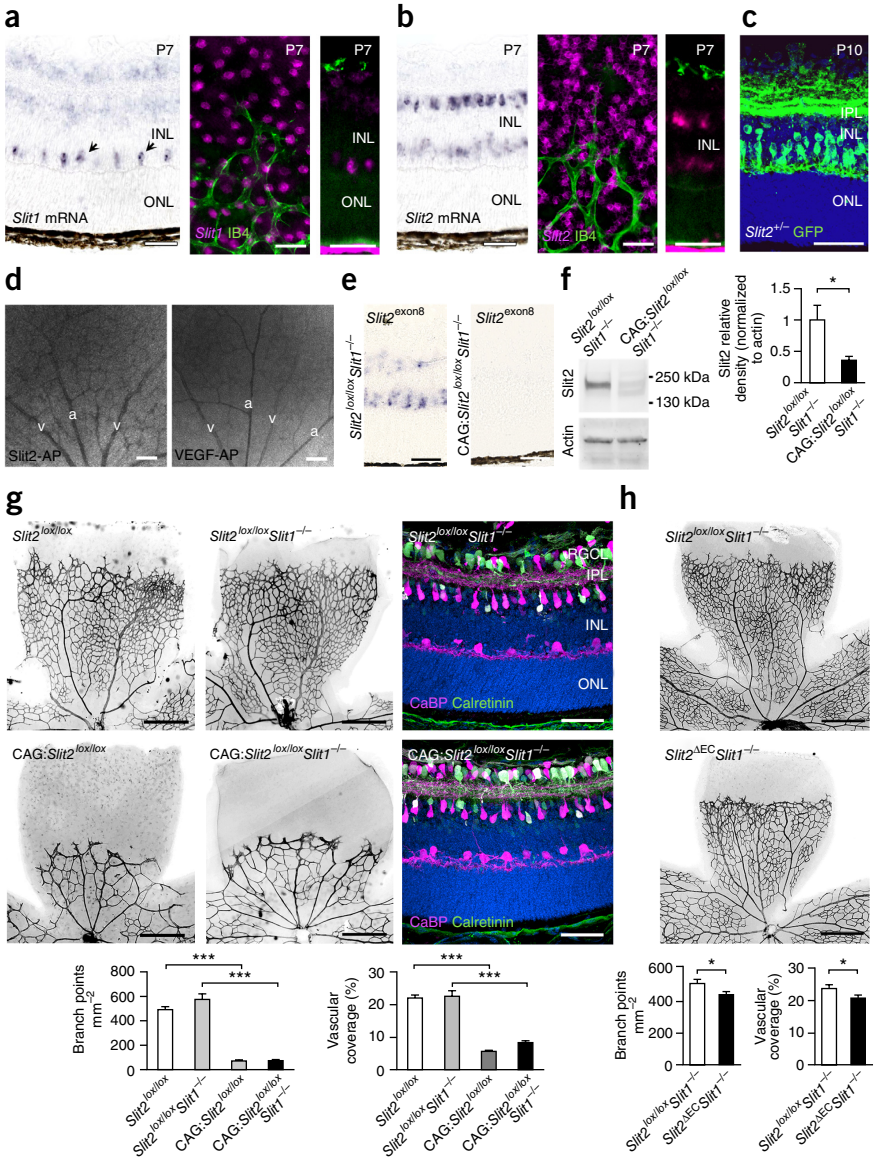

Figure 1 Slit2 promotes retinal angiogenesis. (**a**) *In situ* hybridization for *Slit1* mRNA on a P7 retina section (leftmost and rightmost panels) or flat-mounted retina (middle panel). The vasculature was stained with IB4 (green). The magenta pseudocolor is a negative image of the *in situ* signal. Arrows indicate horizontal cells ($n = 3$ retinas). (**b**) *In situ* hybridization for *Slit2* mRNA on a P7 retina section (leftmost and rightmost panels) or flat-mounted retina (middle panel). The vasculature was stained with IB4 (green) ($n = 2$ retinas). (**c**) Retinal section from *Slit2*$^{+/-}$ mice at P10 stained with anti-GFP ($n = 2$ retinas). (**d**) Binding of Slit2-AP and VEGF-AP to flat-mounted P5 retinas of wild-type mice. The data are representative of nine retinas per condition. v, vein; a, artery. (**e**) *In situ* hybridization (*Slit2* exon 8–specific probe) on P7 retinas of *Slit2*$^{lox/lox}$*Slit1*$^{-/-}$ ($n = 6$) and CAG:*Slit2*$^{lox/lox}$*Slit1*$^{-/-}$ ($n = 11$) mice. For the *Slit2*$^{lox/lox}$*Slit1*$^{-/-}$ and CAG:*Slit2*$^{lox/lox}$*Slit1*$^{-/-}$ mice, tamoxifen was administered at P0. (**f**) Western blot quantification (one retina per lane) of Slit2 expression in P7 retinal extracts from mice injected with tamoxifen at P0 ($n = 3$ *Slit2*$^{lox/lox}$*Slit1*$^{-/-}$ retinas; $n = 11$ CAG:*Slit2*$^{lox/lox}$ *Slit1*$^{-/-}$ retinas; $^{*}P = 0.02$, Mann–Whitney test). (**g**,**h**) Flat-mounts of retinas from P7 *Slit*-knockout mice and control littermates stained with IB4. Branch point density ($n = 24$, 13, 32, 11, 15 and 19 retinas for *Slit2*$^{lox/lox}$, *Slit2*$^{lox/lox}$*Slit1*$^{-/-}$, CAG:*Slit2*$^{lox/lox}$, CAG:*Slit2*$^{lox/lox}$*Slit1*$^{-/-}$, *Slit2*$^{lox/lox}$*Slit1*$^{-/-}$ and *Slit2*$^{\Delta EC}$*Slit1*$^{-/-}$ mice, respectively) and the percentage of vascular coverage ($n = 15$, 15, 16, 11, 11 and 13 retinas for *Slit2*$^{lox/lox}$, *Slit2*$^{lox/lox}$*Slit1*$^{-/-}$, CAG:*Slit2*$^{lox/lox}$, CAG:*Slit2*$^{lox/lox}$*Slit1*$^{-/-}$, *Slit2*$^{lox/lox}$*Slit1*$^{-/-}$ and *Slit2*$^{\Delta EC}$*Slit1*$^{-/-}$ mice, respectively) were determined. Rightmost panels in **g** show sections stained with anti-calretinin (green) and anti-calbindin (CaBP) (magenta) ($n = 2$ *Slit2*$^{lox/lox}$*Slit1*$^{-/-}$ retinas; $n = 3$ CAG:*Slit2*$^{lox/lox}$ *Slit1*$^{-/-}$ retinas). All results are presented as mean ± s.e.m. (also see **Supplementary Table 1**). $^{*}P < 0.05$, $^{***}P < 0.001$, Student's *t*-test. Scale bars, 50 µm in **a**–**c**, **e** and rightmost images in **g**; 150 µm in **d**; and 500 µm in leftmost and middle images in **g** and all panels in **h**. INL, inner nuclear layer; IPL, inner plexiform layer; ONL, outer nuclear layer; RGCL, retinal ganglion cell layer.

and **Supplementary Fig. 2f**). These retinal defects were accompanied by a severe reduction in the total number of endothelial cells labeled with an antibody to the Erg-1/2/3 transcription factors[21] (1,984 ± 138 Erg-1/2/3$^+$ cells in retinas of *Slit2*$^{lox/lox}$*Slit1*$^{-/-}$ mice, versus 347 ± 152 in retinas from CAG:*Slit2*$^{lox/lox}$*Slit1*$^{-/-}$ mice; the number of cells was measured in one 45° retinal wedge; $P < 0.0001$, Student's *t*-test). Moreover, the endothelial cell density in CAG:*Slit2*$^{lox/lox}$*Slit1*$^{-/-}$ mutants was significantly decreased in retinal veins (164 ± 5 Erg-1/2/3$^+$ cells per millimeter of vein in *Slit2*$^{lox/lox}$*Slit1*$^{-/-}$ mice, versus 75 ± 6 in CAG:*Slit2*$^{lox/lox}$*Slit1*$^{-/-}$ mice; $P < 0.001$, Mann–Whitney test), as well as in the vascular plexus (3.7 ± 0.25 Erg-1/2/3$^+$ cells per 50 µm of vessel branch in *Slit2*$^{lox/lox}$*Slit1*$^{-/-}$ mice, versus 1.7 ± 0.23 in CAG:*Slit2*$^{lox/lox}$*Slit1*$^{-/-}$ mice; $P = 0.0012$, Mann–Whitney test). By contrast, immunolabeling of P7 and P12 retinas with various markers of retinal neurons revealed comparable development and structure of the retinal layers in control and CAG:*Slit2*$^{lox/lox}$*Slit1*$^{-/-}$ mutant mice (**Fig. 1g** and **Supplementary Fig. 4a**,**b**). These data show that Slit2 is selectively required for angiogenesis in the postnatal mouse retina.

Although the primary source of Slit2 in the retina is the INL, in humans SLIT2 is also expressed by endothelial cells[15,22], suggesting that endothelial Slits might affect vascular development. We therefore deleted *Slit2* in endothelial cells on a *Slit1*-mutant background and examined retinal vascular development. *Slit2*$^{lox/lox}$*Slit1*$^{-/-}$mice were crossed to mice carrying an endothelial cell–specific and inducible *Cre* allele (*Cdh5*:*Cre*^{ERT2}) to generate *Slit2*$^{\Delta EC}$*Slit1*$^{-/-}$ mice[23,24]. Vascular development was significantly reduced in retinas from *Slit2*$^{\Delta EC}$*Slit1*$^{-/-}$ mice compared to those from *Slit2*$^{lox/lox}$*Slit1*$^{-/-}$ mice ($P = 0.03$ for branch point quantification; $P = 0.02$ for vascular coverage) (**Fig. 1h**), although these defects were much less severe than those observed in CAG:*Slit2*$^{lox/lox}$*Slit1*$^{-/-}$ mice. These data show that Slit2 from multiple tissue sources, including endothelial cells and INL neurons, contributes to retinal vascular development.

Slit2 signals via Robo1 and Robo2 to drive retinal angiogenesis

To determine which Slit receptor (or receptors) mediates Slit2 function in retinal vessels, we analyzed published microarray data from purified mouse P5 retinal endothelial cells[25]. These cells showed the highest expression of *Robo4*; expression of *Robo1* was lower than that of *Robo4*, and there was virtually no *Robo2* expression (**Fig. 2**). Quantitative PCR (qPCR) and western blotting (**Fig. 2b** and **Supplementary Fig. 5**) of primary human endothelial cells (human umbilical vein endothelial cells (HUVECs), human umbilical artery endothelial cells, human dermal microvascular endothelial cells and human retinal microvascular endothelial cells) revealed high ROBO4 levels, ROBO1 levels lower than those of ROBO4 and no detectable ROBO2 (refs. 22,26 and data not shown). Notably, transfection of HUVECs with small interference RNA (siRNA) targeting *ROBO1* led to strongly increased expression of *ROBO2* mRNA and protein, whereas *ROBO4* levels were not affected (**Fig. 2c**,**d**). Likewise, endothelial cells isolated from the lungs of *Robo1*$^{-/-}$ mice showed upregulation of Robo2 (**Fig. 2e**). To completely abrogate expression of ROBO1 and ROBO2 receptors, we used combined siRNA knockdown of *ROBO1* and *ROBO2*, which decreased amounts of both *ROBO1* and *ROBO2* mRNA and encoded protein (**Fig. 2c**,**d**), or we used double-knockout mice deficient in Robo1 and Robo2. As *Robo2*-knockout mice die at birth[27], we intercrossed mice harboring a *Robo2* conditional allele (*Robo2*$^{lox/lox}$)[28] to the *Cdh5*:*Cre*^{ERT2} line (hereinafter referred to as *Robo2*$^{\Delta EC}$). Endothelial cells isolated from the lungs of *Robo1*$^{-/-}$*Robo2*$^{\Delta EC}$ double-knockout mice showed reduced expression of both Robo1 and Robo2 after Cre activation by tamoxifen (**Fig. 2e**).

We next examined Slit binding *in vivo* in retinas of *Robo1*$^{-/-}$, *Robo4*$^{-/-}$ (refs. 7,29) and *Robo1*$^{-/-}$*Robo2*$^{\Delta EC}$ mice. Slit2-AP binding to P5 retinal vessels was strongly decreased in *Robo1*$^{-/-}$*Robo2*$^{\Delta EC}$ mice but was comparable to that in controls in *Robo1*$^{-/-}$ and *Robo4*$^{-/-}$ mice, indicating that Robo1 and Robo2 are the primary Slit receptors on developing vessels (**Fig. 2f**). The residual binding in retinas of *Robo1*$^{-/-}$*Robo2*$^{\Delta EC}$ mice likely reflects the expression of the Robo1 and Robo2 receptors by vessel-associated cells.

We then studied the effects of a loss of *Robo* function on angiogenesis. By staining P5 and P7 retinas with the endothelial-specific lectin IB4, we found that the retinal vasculature developed normally in *Robo1*$^{-/-}$, *Robo2*$^{\Delta EC}$ and *Robo4*$^{-/-}$ mice, similar to what was seen in the compound-heterozygous mice (**Fig. 2h**,**i** and **Supplementary Fig. 6**). In contrast, the number of vessel branch points was significantly reduced in *Robo1*$^{-/-}$*Robo2*$^{\Delta EC}$ mice ($P = 0.0001$), a similar but less severe defect compared to that seen in CAG:*Slit2*$^{lox/lox}$ mice (branch point quantification: 72 for CAG:*Slit2*$^{lox/lox}$, 76 for CAG:*Slit2*$^{lox/lox}$ *Slit1*$^{-/-}$ and 142 for *Robo1*$^{-/-}$*Robo2*$^{\Delta EC}$ mice). This defect was not aggravated further in *Robo1*$^{-/-}$*Robo2*$^{\Delta EC}$*Robo4*$^{-/-}$mice (**Fig. 2g–i** and **Supplementary Fig. 6**). As with CAG:*Slit2*$^{lox/lox}$ mice, immunolabeling with neuron markers in retinas of *Robo1*$^{-/-}$*Robo2*$^{\Delta EC}$ mice revealed a retinal layer structure comparable to that of controls at P7 and P15 (**Fig. 2g** and **Supplementary Fig. 4c**,**d**). At P7, both the total number of endothelial cells in the retina (1,376 ± 114 Erg-1/2/3$^+$ cells in *Robo1*$^{-/-}$*Robo2*$^{lox/lox}$ versus 1,064 ± 79 in *Robo1*$^{-/-}$*Robo2*$^{\Delta EC}$; the number of cells was measured in one 45° retinal wedge; $P = 0.03$, *t*-test) and the density of endothelial cells in veins (169 ± 13 Erg-1/2/3$^+$ cells per millimeter of vein in *Robo1*$^{-/-}$*Robo2*$^{lox/lox}$ versus 110 ± 8 in *Robo1*$^{-/-}$*Robo2*$^{\Delta EC}$; $P = 0.009$, Mann–Whitney test) and vascular plexus (4.68 ± 0.26 Erg-1/2/3$^+$ cells per 50 µm of vessel branch in *Robo1*$^{-/-}$*Robo2*$^{lox/lox}$ versus 2.68 ± 0.16 in *Robo1*$^{-/-}$*Robo2*$^{\Delta EC}$; $P = 0.0025$, Mann–Whitney test) were significantly reduced in *Robo1*$^{-/-}$*Robo2*$^{\Delta EC}$ mice. Together, these data show that Slit2 signaling through Robo1 promotes angiogenesis *in vivo* and that endothelial Robo2, but not Robo4, compensates for the absence of Robo1.

Angiogenic defects in *Robo1*$^{-/-}$*Robo2*$^{\Delta EC}$ mice were somewhat less severe than those in CAG:*Slit2*$^{lox/lox}$*Slit1*$^{-/-}$ mice, suggesting that Slit2 also affects the development of vascular cell types such as pericytes, smooth muscle cells and leukocytes, and it has been reported that these cell types respond to Slit2 *in vitro*[13,22,30]. To determine whether Slit2 signaling in one or more of these cell types requires Robo1 and Robo2, we generated CAG:*Robo2*$^{lox/lox}$*Robo1*$^{-/-}$ mice. IB4 staining showed that the extent of vascular development was severely reduced in retinas from CAG:*Robo2*$^{lox/lox}$*Robo1*$^{-/-}$ mice, phenocopying retinas from CAG:*Slit2*$^{lox/lox}$*Slit1*$^{-/-}$ mice (**Fig. 2j**). Overall, these data suggest that Slit2 signals through Robo1 and Robo2 on endothelial cells and other vessel-associated cell types to promote angiogenesis.

Robo1 and Robo2 control Slit2- and VEGF-A–induced endothelial cell migration

To characterize endothelial cell behavior in *Slit*- and *Robo*-knockout mice, we examined endothelial cell proliferation by injecting 5-ethynyl-2-deoxyuridine (EdU) into P3 and P7 mice. Retinas were collected 2 h after the EdU pulse and stained with IB4 and anti–Erg-1/2/3, and the number of stained cells was quantified (see Online Methods and **Supplementary Fig. 7a**)[31]. At P3 and P7, the percentage of proliferating endothelial cells in retinas (the percentage of Erg-1/2/3$^+$ cells that were labeled with EdU) was not significantly different between *Robo1*$^{-/-}$*Robo2*$^{lox/lox}$ and *Robo1*$^{-/-}$*Robo2*$^{\Delta EC}$ mice (**Fig. 3a**; 18.86% ± 1.34% in retinas from P3 *Robo1*$^{-/-}$*Robo2*$^{lox/lox}$ mice versus 16.09% ± 3.34% in retinas from P3

Robo1$^{-/-}$*Robo2*$^{\Delta EC}$ mice; 11.20% ± 0.98% in retinas from P7 *Robo1*$^{-/-}$ *Robo2*$^{lox/lox}$ mice versus 12.13% ± 0.78% in retinas from P7 *Robo1*$^{-/-}$ *Robo2*$^{\Delta EC}$ mice; no significant results via Mann–Whitney test). In *Slit1*- and *Slit2*-knockout mice, the percentage of proliferating endothelial cells was also similar to that in controls at P7 (**Fig. 3a**; 13.25% ± 1.29% in retinas from *Slit2*$^{lox/lox}$*Slit1*$^{-/-}$ mice versus 13.22% ± 2.56% in those from CAG:*Slit2*$^{lox/lox}$*Slit1*$^{-/-}$ mice; no significant results via *t*-test), but it was significantly reduced at P3 (31% ± 2.16% in retinas from *Slit2*$^{lox/lox}$*Slit1*$^{-/-}$ mice versus 11.00% ± 1.16% in those from CAG:*Slit2*$^{lox/lox}$*Slit1*$^{-/-}$ mice; $P = 0.0079$, Mann–Whitney test). We next measured the percentage of proliferating endothelial cells at the front of the growing retinal vasculature. At P3 and P7, this parameter was normal in *Robo1*- and *Robo2*-knockout mice but was significantly reduced in *Slit1*- and *Slit2*-knockout mice ($P = 0.016$ and $P = 0.0025$ at P3 and P7, respectively; **Supplementary Fig. 7a**). These data show that Slits influence endothelial cell proliferation *in vivo*. However, *in vitro* studies showed that neither Slit2 treatment

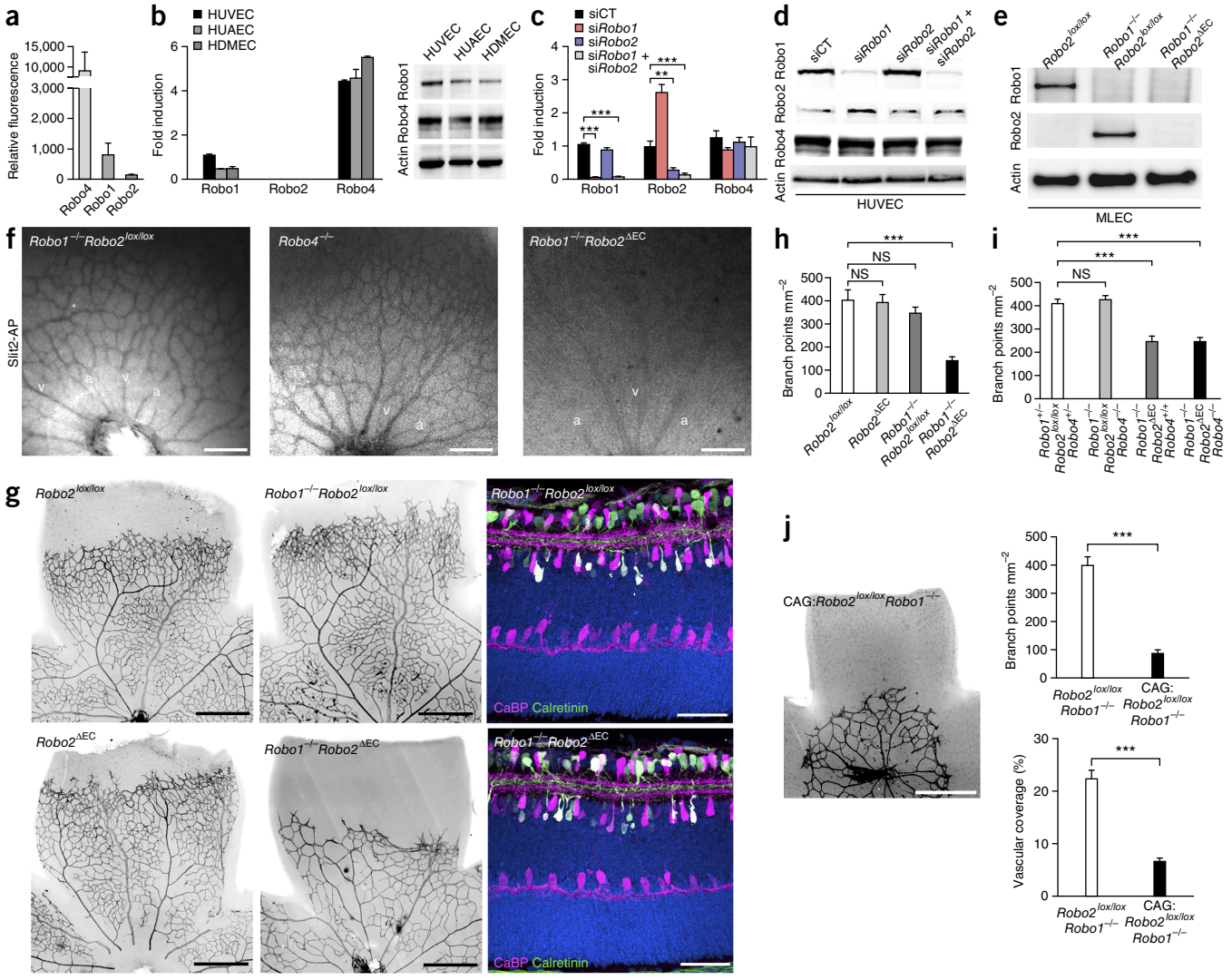

Figure 2 Abnormal retinal angiogenesis in *Robo1*- and *Robo2*-knockout mice. (**a**,**b**) Robo expression as assessed by microarray analysis of mouse retinal endothelial cells (**a**), qPCR analysis of human endothelial cell mRNA (**b**, left) and western blot of the corresponding human endothelial cells (**b**, right). Results shown are from three independent experiments. HUVEC, human umbilical vein endothelial cell; HUAEC, human umbilical artery endothelial cell; HDMEC, human dermal microvascular endothelial cell. (**c**–**e**) Robo expression after *Robo* knockdown in HUVECs as determined by qPCR (**c**; $^{**}P < 0.01$, $^{***}P < 0.001$ compared to scrambled siRNA control (siCT)) and western blot (**d**) and in mouse lung endothelial cells (MLEC) isolated from *Robo1Robo2*–double-knockout mice as determined by western blot (**e**) (two experiments for each group in **d** and **e**). siRobo, siRNA targeting the indicated Robo protein. (**f**) Slit2-AP binding on P5 retinal flat-mounts from *Robo*-knockout mice ($n = 7$, $n = 2$ and $n = 11$ retinas for *Robo1*$^{-/-}$*Robo2*$^{lox/lox}$, *Robo4*$^{-/-}$ and *Robo1*$^{-/-}$*Robo2*$^{\Delta EC}$ mice, respectively). v, vein; a, artery. (**g**) Retinal flat-mounts of P7 *Robo1*- and *Robo2*-knockout mice and control mice stained with IB4. Rightmost panels show sections stained with anti-calretinin (green) and anti-CaBP (magenta; $n = 3$ *Robo1*$^{-/-}$*Robo2*$^{lox/lox}$ retinas; $n = 6$ *Robo1*$^{-/-}$*Robo2*$^{\Delta EC}$ retinas). (**h**,**i**) Quantification of branch point density ($n = 10$, 23, 21 and 21 retinas for *Robo2*$^{lox/lox}$, *Robo1*$^{-/-}$*Robo2*$^{lox/lox}$, *Robo2*$^{\Delta EC}$ and *Robo1*$^{-/-}$*Robo2*$^{\Delta EC}$ mice, respectively (**h**); $n = 12$, 8, 8 and 6 retinas for *Robo1*$^{+/-}$*Robo2*$^{lox/lox}$*Robo4*$^{+/-}$, *Robo1*$^{-/-}$*Robo2*$^{lox/lox}$*Robo4*$^{-/-}$, *Robo1*$^{-/-}$*Robo2*$^{\Delta EC}$*Robo4*$^{+/+}$ and *Robo1*$^{-/-}$*Robo2*$^{\Delta EC}$*Robo4*$^{-/-}$ mice, respectively (**i**)). (**j**) Representative flat-mount of retina from P7 CAG:*Robo2*$^{lox/lox}$*Robo1*$^{-/-}$ mouse stained with IB4. Branch point density and the percentage of vascular coverage were quantified ($n = 6$ *Robo2*$^{lox/lox}$*Robo1*$^{-/-}$ retinas; $n = 20$ CAG:*Robo2*$^{lox/lox}$*Robo1*$^{-/-}$ retinas). All results are presented as mean ± s.e.m. $^{***}P < 0.001$, Student's *t*-test (**h**) or Mann–Whitney test (**i**,**j**). NS, not significant. Controls used for comparison were *Robo2*$^{lox/lox}$ (**h**) and *Robo1*$^{+/-}$*Robo2*$^{lox/lox}$*Robo4*$^{+/-}$ (**i**). Scale bars, 200 μm in **f**, 500 μm in leftmost and middle images in **g** and in **j**, and 50 μm in rightmost images in **g**.

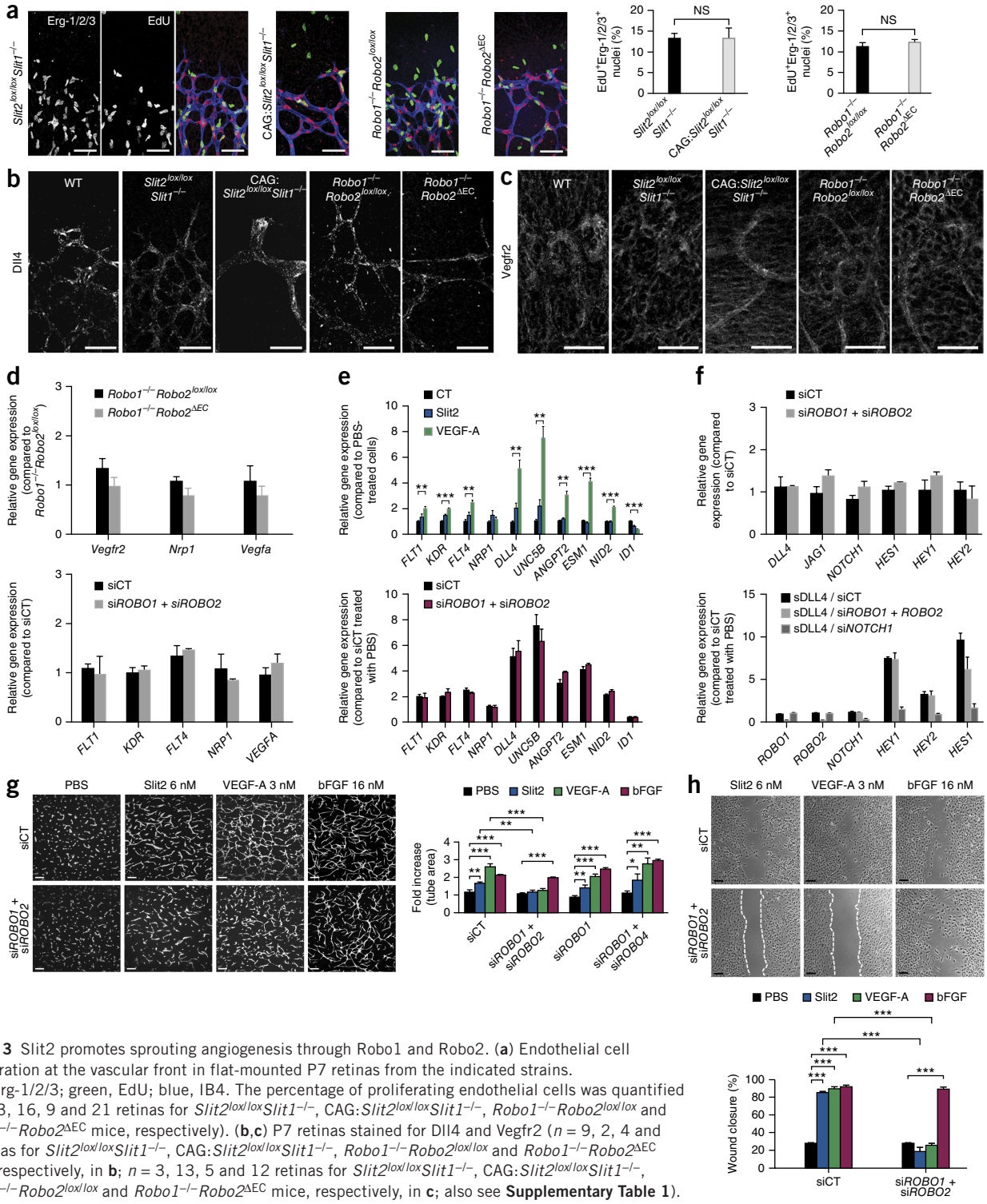

Figure 3 Slit2 promotes sprouting angiogenesis through Robo1 and Robo2. (**a**) Endothelial cell proliferation at the vascular front in flat-mounted P7 retinas from the indicated strains. Red, Erg-1/2/3; green, EdU; blue, IB4. The percentage of proliferating endothelial cells was quantified (n = 13, 16, 9 and 21 retinas for *Slit2*$^{lox/lox}$*Slit1*$^{-/-}$, CAG:*Slit2*$^{lox/lox}$*Slit1*$^{-/-}$, *Robo1*$^{-/-}$*Robo2*$^{lox/lox}$ and *Robo1*$^{-/-}$*Robo2*$^{\Delta EC}$ mice, respectively). (**b**,**c**) P7 retinas stained for Dll4 and Vegfr2 (n = 9, 2, 4 and 6 retinas for *Slit2*$^{lox/lox}$*Slit1*$^{-/-}$, CAG:*Slit2*$^{lox/lox}$*Slit1*$^{-/-}$, *Robo1*$^{-/-}$*Robo2*$^{lox/lox}$ and *Robo1*$^{-/-}$*Robo2*$^{\Delta EC}$ mice, respectively, in **b**; n = 3, 13, 5 and 12 retinas for *Slit2*$^{lox/lox}$*Slit1*$^{-/-}$, CAG:*Slit2*$^{lox/lox}$*Slit1*$^{-/-}$, *Robo1*$^{-/-}$*Robo2*$^{lox/lox}$ and *Robo1*$^{-/-}$*Robo2*$^{\Delta EC}$ mice, respectively, in **c**; also see **Supplementary Table 1**). WT, wild type. (**d**) Expression of *Vegfr2* (*Kdr*), *Nrp1* and *Vegfa* as determined by qPCR in endothelial cells isolated from *Robo1*$^{-/-}$*Robo2*$^{\Delta EC}$ mice (upper panel) and in HUVECs with si*ROBO1* and si*ROBO2* compared to scrambled siRNA controls (siCT, lower panel). (**e**) Tip cell marker gene expression analysis by qPCR of HUVECs treated for 20 h with Slit2 or VEGF-A (upper panel, compared to PBS control (CT)) and of VEGF-A–treated HUVECs after application of scrambled control siRNA or knockdown of *ROBO1* and *ROBO2* (lower panel, compared to PBS control). $^{**}P < 0.01$, $^{***}P < 0.001$. (**f**) Expression of NOTCH signaling molecules in HUVECs with knockdown of *ROBO1* and *ROBO2* or of *NOTCH1* determined by qPCR (upper panel) and after sDLL4 stimulation (lower panel). (**g**) HUVEC sprouting in 3D fibrin gels (left) and quantification (right). Cells were treated with siRNAs and then with recombinant proteins as indicated for 96 h. $^{*}P < 0.05$, $^{**}P < 0.01$, $^{***}P < 0.001$ compared to PBS-treated control. (**h**) HUVEC scratch-wound migration assay (left) and quantification (right). Cells were treated with siRNAs and then with recombinant proteins as indicated for 16 h. Dashed lines mark wound migration edges. $^{***}P < 0.001$ compared to PBS-treated control. All results are presented as mean ± s.e.m. as determined via Student's t-test (**a**) or two-way analysis of variance and Tukey's multiple-comparisons test (n = 3 independent experiments in **d**–**h**). NS, not significant. Scale bars, 50 µm in **a**–**c**, 180 µm in **g** and **h**.

nor knockdown of *ROBO1* and *ROBO2* affected HUVEC proliferation (**Supplementary Fig. 8a–d**). Moreover, the reduced extent of the vasculature was not due to an increase in endothelial cell apoptosis, as assessed by TUNEL staining (**Supplementary Fig. 7b**,**c**).

We next tested the expression of a battery of molecules regulating angiogenesis in CAG:*Slit2*$^{lox/lox}$*Slit1*$^{-/-}$ and *Robo1*$^{-/-}$*Robo2*$^{\Delta EC}$ mice and in littermate controls. We detected similar expression of Plexin-D1 and Neuropilin-1, two other axon-guidance receptors involved in angiogenesis[32], in mutant and control mice (**Supplementary Fig. 8e**,**f**). Immunostaining for Collagen IV and IB4 showed no increase in the number of retracted sprouts or collapsed vessels in retinas from *Robo1*$^{-/-}$*Robo2*$^{\Delta EC}$ and CAG:*Slit2*$^{lox/lox}$*Slit1*$^{-/-}$ mice, indicating that vessel stability was not perturbed (**Supplementary Fig. 8g**,**h**). Moreover, VEGF-A expression was unaffected in the retinas of *Robo1*$^{-/-}$*Robo2*$^{\Delta EC}$ and CAG:*Slit2*$^{lox/lox}$*Slit1*$^{-/-}$ mice (data not shown). Likewise, expression of the Notch ligand Delta-like 4 (Dll4) and of VEGF receptor 2 (Vegfr2) was comparable to that in control retinas (**Fig. 3b**,**c**). Confirming the *in vivo* immunostaining results, qPCR analysis of endothelial cells isolated from *Robo1*$^{-/-}$*Robo2*$^{\Delta EC}$ mice or of HUVECs in which *ROBO1* and *ROBO2* were knocked down showed no effects on the expression levels of VEGF and VEGF receptors (**Fig. 3d**). VEGF signaling induces the expression of *DLL4*, *UNC5B*, *ANGPT2*, *ESM1* and *NID2* (refs. 25,33–36). VEGF-driven expression of these genes was not altered by knockdown of *ROBO1* and *ROBO2*, and Slit2 treatment of HUVECs did not induce their expression (**Fig. 3e**). Moreover, knockdown of *ROBO1* and *ROBO2* did not alter the expression of NOTCH pathway components, and NOTCH target gene expression induced by DLL4 was similar in control HUVECs and in cells with *ROBO1*- or *ROBO2*-knockdown, whereas *NOTCH1*-knockdown abolished NOTCH target gene expression (**Fig. 3f**).

These data suggest that Slit2 drives angiogenic sprouting and endothelial cell migration primarily via ROBO1 and ROBO2. In an *in vitro* sprouting assay in which HUVECs were embedded within a 3D fibrin gel[37], nanomolar concentrations of recombinant Slit2 robustly induced angiogenic sprouting, and this effect was abolished by combined knockdown of *ROBO1* and *ROBO2*, but not by knockdown of *ROBO1*, *ROBO2* or *ROBO4* singly or by combined knockdown of *ROBO1* and *ROBO4* (**Fig. 3g** and **Supplementary Fig. 9e**). These data support the hypothesis that Slit2 acts primarily through ROBO1 and ROBO2.

Notably, sprouting angiogenesis induced by VEGF-A also required the presence of ROBO1 and ROBO2 (**Fig. 3g**). Overexpression of miR-218, which targets the 3′ UTRs of *ROBO1* and *ROBO2* mRNAs and prevents the expression of both receptors[38,39], also inhibited Slit2- and VEGF-A–induced sprouting (**Supplementary Fig. 9a–d**). Sprouting in response to VEGF was not affected by single knockdown of *ROBO1*, *ROBO2* or *ROBO4* or by combined knockdown of *ROBO1* and *ROBO4* (**Fig. 3g** and **Supplementary Fig. 9e**), confirming that only the combined knockdown of *ROBO1* and *ROBO2* affects VEGF-A–induced sprouting. Combined knockdown of *ROBO1* and *ROBO2* also severely inhibited cell migration in response to Slit2 and VEGF-A in a scratch-wound migration assay (**Fig. 3h**). In contrast, bFGF-induced sprouting and migration were unaffected by combined knockdown of *ROBO1* and *ROBO2* (**Fig. 3g**,**h**).

Slit2- and VEGF-induced RAC1 activation requires ROBO1 and ROBO2

The unexpected cross-talk that we observed between VEGF or Slit2 signaling and Robo1 and Robo2 signaling in endothelial cell migration prompted us to determine the molecular mechanisms

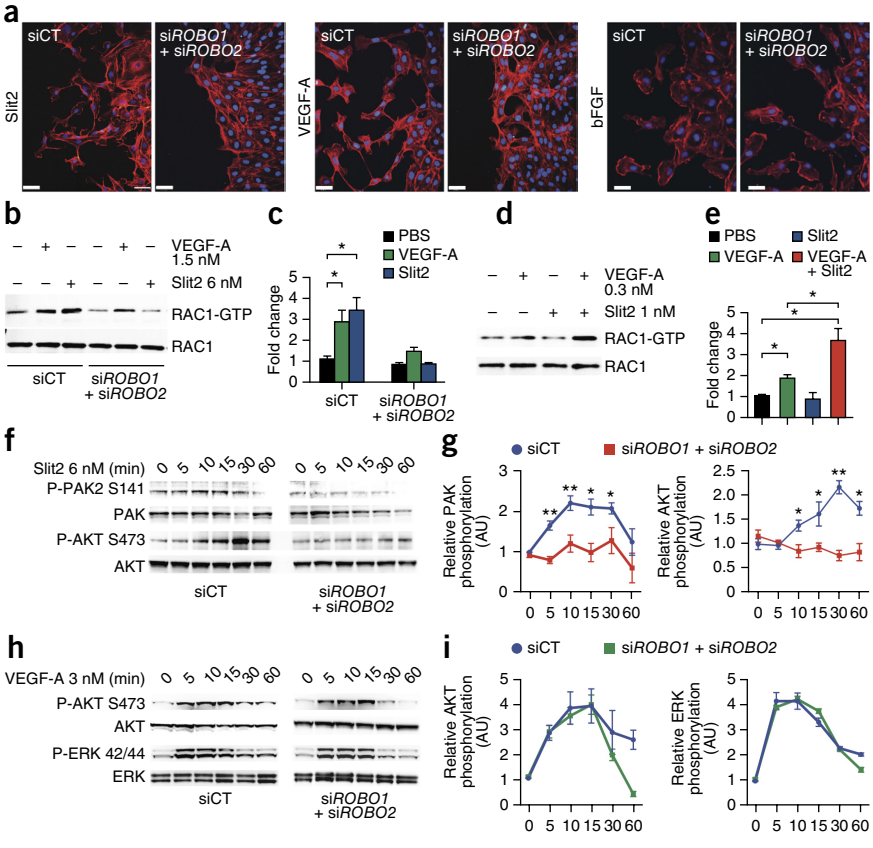

Figure 4 ROBO1 and ROBO2 regulate Slit2- and VEGF-A–induced RAC1 activation. (**a**) Phalloidin (red) and DAPI (blue) staining of HUVECs at the edge (left-hand side of all images) of a scratch wound 16 h after wounding. Cells were treated with siRNAs and then with recombinant proteins as indicated. Cells treated with siRNAs targeting *ROBO1* and *ROBO2* did not form lamellipodia in response to Slit2 and VEGF, but formation did occur in response to bFGF. Scale bars, 45 µm. (**b**,**c**) RAC1-GTP loading induced by Slit2 and VEGF in HUVECs with control siRNA and with siRNA targeting *ROBO1* and *ROBO2* (5-min stimulation) (**b**). The results of three independent experiments were quantified (**c**). $^{*}P < 0.05$ compared to PBS-treated control. (**d**,**e**) Effects of low-dose Slit2 and VEGF treatment on RAC1-GTP loading (5-min stimulation) (**d**). The results of three experiments were quantified (**e**). $^{*}P < 0.05$ compared to PBS-treated control. (**f**,**g**) Effects of Slit2 treatment on PAK2 and AKT phosphorylation in siRNA control HUVECs and cells with knockdown of *ROBO1* and *ROBO2* (**f**). The results of three independent experiments were quantified (**g**). $^{*}P < 0.05$, $^{**}P < 0.01$ compared to PBS-treated control. (**h**,**i**) Effects of VEGF-A on phosphorylation of ERK and AKT in HUVECs with control siRNA and with siRNA targeting *ROBO1* and *ROBO2* (**h**). Quantification of p-AKT compared to total AKT and p-ERK compared to total ERK was performed for three independent experiments (**i**). All values are mean ± s.e.m. *P* values were calculated using Student's *t*-test.

underlying the interaction between these signaling pathways. High magnification of migrating endothelial cells at the edges of scratch wounds showed that combined knockdown of *ROBO1* and *ROBO2* suppressed Slit2- or VEGF-A–induced lamellipodia formation (**Fig. 4**). As lamellipodia formation requires the activation of RAC1 (ref. 40), we asked whether RAC1 was activated downstream of ROBO1 and ROBO2 in response to Slit2 and VEGF-A. Slit2 and VEGF-A activated RAC1 in HUVECs and in lung endothelial cells, and this effect was lost in HUVECs with knockdown of *ROBO1* and *ROBO2* and in lung endothelial cells isolated from double-knockout mice deficient in Robo1 and Robo2; in contrast, RAC1 activation was not affected in lung endothelial cells from *Robo1*- or *Robo4*-knockout mice (**Fig. 4b**,**c** and **Supplementary Fig. 10a**–**c**). Slit2 treatment also activated phosphorylation of the RAC1 target p21-activated kinase (PAK) in a ROBO1- and ROBO2-dependent manner (**Fig. 4f**,**g** and **Supplementary Fig. 10f**,**g**). Low-dose VEGF-A together with Slit2 cooperatively enhanced RAC-GTP loading in HUVEC cells (**Fig. 4d**,**e**). Taken together, these results demonstrate synergistic RAC1 activation by VEGF-A and Slit2.

The combined loss of *Robo1* and *Robo2*, but not the loss of *Robo1* or *Robo4* alone, also abolished Slit2-mediated AKT activation (**Supplementary Fig. 10d**,**e**,**g**). However, the combined loss of *Robo1* and *Robo2* did not affect the activation of AKT or ERK in response to VEGF-A, and the administration of low-dose VEGF-A with Slit2 did not show a cooperative effect on AKT activation (**Fig. 4h**,**i** and **Supplementary Fig. 10h**,**i**). Thus, Slit2–Robo1 and Slit2–Robo2 signaling selectively target VEGF-A–induced RAC1 activation, which is required for cytoskeletal remodeling, in contrast to the VEGF-A effector pathways that promote cell proliferation and survival.

Previous studies have demonstrated the inhibition of VEGF-A–mediated signaling events after pretreatment with Slit2 (refs. 9,10). Indeed, we found that VEGF-A stimulation following pretreatment with Slit2 led to reduced PAK phosphorylation (**Supplementary Fig. 11a**,**b**). We reasoned that effects on VEGFR2 internalization could explain these disparate results. In accordance with this hypothesis, pretreatment of HUVECs with Slit2 for 5–30 min led to robust VEGFR2 internalization, an effect that was abolished by combined knockdown of *ROBO1* and *ROBO2* (**Supplementary Fig. 11c**,**d**). Thus, pretreatment with Slit2 can antagonize VEGF-A signaling, whereas combined treatment with Slit2 and VEGF-A enhances the signaling events required for endothelial cell migration. These results suggest that interactions between the Slit2 and VEGF pathways through effects on receptor trafficking may be relevant *in vivo* for pro- or anti-migratory signals.

Figure 5 Targeting Slit2–Robo signaling blocks angiogenesis in OIR. (**a**,**c**,**e**,**g**) IB4-stained flat-mounts of P17 retinas from *Slit*-knockout (**a**,**c**) and *Robo*-knockout (**e**) mice after OIR. Retinas in **g** are from mice injected with adenovirus encoding GFP (adCTL) or adenovirus encoding ROBO1-Fc (adROBO1-Fc). A higher-magnification image of neovessel sprouting and vascular tufts is shown in **c**; images show areas indicated by the arrows (upper panels) and arrowheads (lower panels) in **a**. (**b**) Quantification of the avascular area in *Slit*-knockout mice ($n = 10$, 22, 12 and 23 retinas for $Slit2^{lox/lox}$, $Slit2^{lox/lox}Slit1^{-/-}$, CAG:$Slit2^{lox/lox}$ and CAG:$Slit2^{lox/lox}Slit1^{-/-}$ mice, respectively). (**d**) Quantification of neovessel sprouting from veins. (**f**) Quantification of avascular area in *Robo*-knockout mice ($n = 31$, $Robo2^{lox/lox}Robo1^{-/-}$ retinas; $n = 22$, CAG:$Robo2^{lox/lox}Robo1^{-/-}$ retinas). (**h**) Quantification of the avascular area in mice injected with adenovirus encoding GFP ($n = 10$ retinas) or adenovirus encoding ROBO1-Fc ($n =$ 8 retinas). All results are presented as mean ± s.e.m. $^{***}P < 0.001$, Student's *t*-test. NS, not significant. Scale bars, 500 μm in **a**, **e** and **g**; 100 μm in **c**.

Targeting Slit–Robo pathways can inhibit pathological angiogenesis

To determine whether Slit and Robo signaling might have relevance to ocular neovascular diseases, we used a mouse model of oxygen-induced retinopathy (OIR). In this model, pathological sprouting and the formation of leaky vascular tufts occur, mimicking vision-threatening defects seen in subjects with AMD[41]. At P7, $Slit2^{lox/lox}$, $Slit2^{lox/lox}Slit1^{-/-}$, CAG:$Slit2^{lox/lox}$, CAG:$Slit2^{lox/lox}Slit1^{-/-}$, $Robo2^{lox/lox}Robo1^{-/-}$, CAG:$Robo2^{lox/lox}Robo1^{-/-}$ and $Robo1^{-/-}Robo2^{\Delta EC}$ littermate mice were exposed to 75% oxygen for 5 d (until P12) and then maintained in ambient air (normoxia) until P17, to allow pathological neovascularization to set in (**Supplementary Fig. 12**). We induced tamoxifen-mediated gene deletion during the neovascularization period (P12–P17). The extent of vascular regression at P12 was similar in controls and mutants (**Supplementary Fig. 12a**–**f**). *Slit2* expression at P17 was still restricted to the INL and was not upregulated in the retina (**Supplementary Fig. 12j**–**l**). However, quantification at P17 showed a significant increase in the size of the avascular area in CAG:$Slit2^{lox/lox}$ and CAG:$Slit2^{lox/lox}Slit1^{-/-}$ mice compared to $Slit2^{lox/lox}$ and $Slit2^{lox/lox}Slit1^{-/-}$ mice ($P = 0.0001$) (**Fig. 5a**,**b**), demonstrating efficient inhibition of angiogenesis in the absence of *Slit2*. Strikingly, the number of vessel sprouts and pathological neovascular tufts was strongly diminished in CAG:$Slit2^{lox/lox}$ and CAG:$Slit2^{lox/lox}Slit1^{-/-}$ retinas ($P = 0.0009$ and $P = 0.0001$, respectively)

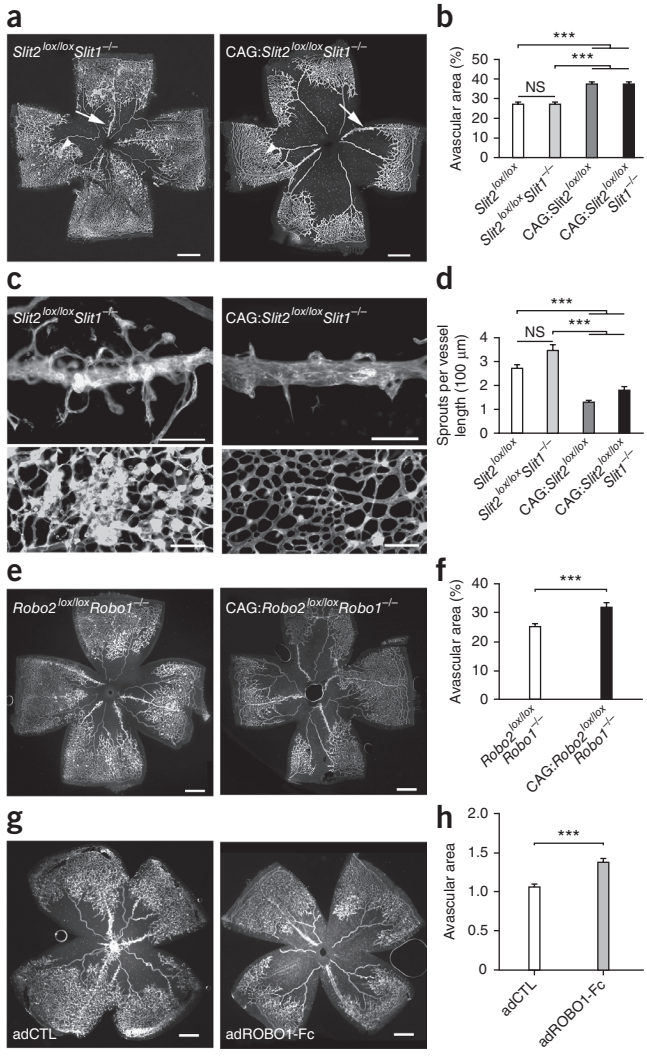

(**Fig. 5c**,**d**). The reduction in the avascular area was not accompanied by increased endothelial cell death or by disorganization of the neural retina (**Supplementary Fig. 13** and data not shown). Notably, a similar reduction in the avascular area and of the number of vessel tufts was also observed in CAG:*Robo2*$^{lox/lox}$*Robo1*$^{-/-}$ mice (**Fig. 5e**,**f**). The number of vessel sprouts was also significantly diminished in retinas from CAG:*Robo2*$^{lox/lox}$*Robo1*$^{-/-}$ mice (1.22 ± 0.16 per 100 µm of vessel length) compared to those from *Robo2*$^{lox/lox}$*Robo1*$^{-/-}$ mice (3.05 ± 0.17; $P < 0.0001$). In contrast, the extent of vascular regression was not affected in *Robo1*$^{-/-}$*Robo2*$^{\Delta EC}$ mice (**Supplementary Fig. 12g–i**). To further explore the efficacy of Slit2 blockade, we treated mice with a control adenovirus encoding GFP or an adenovirus encoding a recombinant protein containing the first two immunoglobulin domains of Robo1 and the immunoglobulin Fc domain (Robo1-Fc) that sequesters Slit2 (ref. 26). Administration of Robo1-Fc was done at P12 and P13, during the neovascularization period (P12–P17). Robo1-Fc–treated mice showed severely reduced angiogenesis and vascular tuft formation (**Fig. 5g**,**h**). Therefore, deletion of *Slit2*, deletion of *Robo1* and *Robo2* or treatment with a Slit trap can reduce pathological neovascularization, indicating that blocking Slit ligand binding to Robo1 and Robo2 receptors might be therapeutically beneficial for individuals with ocular vasoproliferative diseases.

DISCUSSION

The data shown here provide clear genetic evidence for a requisite and selective role of Slit2 signaling through Robo1 and Robo2 in promoting developmental and pathological ocular neovascularization. Slit2 signaling through Robo1 has been shown to stimulate tumor angiogenesis and lymphangiogenesis[26], indicating that pro-angiogenic effects of Slit–Robo1 signaling may also occur in other developmental and pathological contexts. However, Slit–Robo signaling in cancer is complicated by the fact that tumor cells themselves express proteins in the Slit and Robo families, and Slit signaling has been shown to either prevent or enhance tumor cell migration, depending on the experimental setting[42]. Therefore, more work is required before effects of Slit–Robo signaling on tumor angiogenesis can be completely understood.

We show that Slit2 promoted retinal angiogenesis by signaling through Robo1 and Robo2 on endothelial cells and on other vessel-associated cell types. These may include pericytes, smooth muscle cells and leukocytes, all of which respond to Slit2 *in vitro*[13,22,30]. It remains to be determined in precisely which cell types Slit2 signaling is required and how such signaling affects retinal neovascularization. However, our genetic data clearly show that the angiogenic defects in retinas from CAG:*Robo2*$^{lox/lox}$*Robo1*$^{-/-}$ mice were similar to those in retinas from CAG:*Slit2*$^{lox/lox}$ mice in the context of both development and OIR, demonstrating that Slit2 promotes angiogenesis through Robo1 and Robo2, independently of Robo4.

Notably, the severe vascular phenotype of CAG:*Slit2*$^{lox/lox}$ mice occurred without detectable alterations in cell death or vessel stability. In endothelial cells, Slit2 signaling through Robo1 and Robo2 seems to primarily affect migration and sprouting. In support of this idea, neither our study nor previous work[9,26] showed mitogenic activity of Slit2 on endothelial cells. Thus, as in axons, leukocytes and tumor cells, Slit2 signaling in endothelial cells primarily targets cellular motility. However, endothelial cell proliferation, in particular at the vascular front, was reduced in *Slit1* and *Slit2* mutants. Together with impaired endothelial cell motility, this reduction in endothelial cell proliferation resulted in a significant reduction in the number of endothelial cells in the retina. As endothelial cell proliferation appeared to be normal in endothelial-specific *Robo1* and *Robo2* mutants, it is likely that the reduction in cell proliferation was due to Slit activity on vessel-associated cell types such as mural cells or leukocytes. Given that the severe defects in vascular growth and branching in CAG:*Slit2*$^{lox/lox}$ mice were phenocopied in CAG:*Robo2*$^{lox/lox}$*Robo1*$^{-/-}$ mice, it is likely that Slit2 activity on endothelial cell proliferation is also mediated by Robo1 and Robo2.

At the molecular level, Slit2 activation of downstream signals, including AKT and RAC1 signaling, was abolished by the inactivation of *ROBO1* and *ROBO2*, indicating that decreased activity of these signaling proteins may contribute to defective sprouting and/or cell migration *in vivo*. Notably, ROBO1 and ROBO2 also seemed to be required for RAC1 activation and lamellipodia formation in response to VEGF, whereas these receptors did not affect the activation of ERK and AKT by VEGF. The mechanistic details of these effects remain to be elucidated, but the data suggest that signaling between Slit2 and Robo1 or Robo2 is a critical environmental signal for retinal endothelial cell migration.

In *Vegfr2* (*Kdr*) mutants, retinal angiogenesis fails[43], indicating that Slit2 cannot promote migration in the absence of VEGF signaling. In the absence of Slit2 signaling, VEGF fails to induce RAC1 activation; however, AKT and ERK activation remains intact. Thus, inhibition of Slit2 signaling blocks VEGF-induced endothelial cell migration and angiogenesis, but cell survival and ERK-driven expression of DLL4 and NOTCH activation are not affected. The expression pattern of Slit2 and VEGF in retinas *in vivo* provides insight into the sites of combined pathway activation. We found that Slit2 was produced in bipolar neurons located beneath the vascular plexus. VEGF is produced by hypoxic astrocytes ahead of the vascular plexus and is downregulated in vascularized tissue via a HIF1-dependent negative feedback loop[44]. Thus, we propose that endothelial cells in the vascular plexus are exposed to Slit2, but not to VEGF. Pretreatment of HUVECs with Slit2 inhibited VEGF signaling by promoting VEGFR2 internalization, indicating that Slit2 may provide another feedback loop to limit VEGF signaling in already vascularized tissues. In contrast, endothelial cells at the vascular front are likely to experience combined Slit2 and VEGF activation, in turn activating migration. The dual ability of Slit2–Robo1 and Slit2–Robo2 signaling to either promote or prevent VEGF signaling resolves currently conflicting data regarding both pro- and anti-angiogenic activities of Slit2. It would be interesting to determine whether the effects of Slit2 on vessel permeability also involve only Robo1 and Robo2, or whether Robo4 is also involved.

In conclusion, the data shown here reveal a previously unanticipated role for Slit signaling through Robo1 and Robo2 in angiogenic sprouting and provide a rationale for developing blocking strategies to inhibit neovascularization, particularly in individuals who are resistant to anti-VEGF therapies.

METHODS

Methods and any associated references are available in the online version of the paper.

Note: Any Supplementary Information and Source Data files are available in the online version of the paper.

ACKNOWLEDGMENTS

This project was supported by grants from the Agence Nationale de la Recherche (ANR; ANR-11BSV102502 to A.C. and A.E.), the Fondation pour la Recherche Médicale ("Programme Équipe FRM" to A.C.; DEQ20120323700), Sanofi-Fovea (to A.C.), Fondation Leducq (Artemis Transatlantic Network of Excellence, to A.E.) and the Thome Foundation for Age-Related Macular Degeneration (to A.E.). It was performed in the frame of the LABEX LIFESENSES (reference ANR-10-LABX-65),

supported by French state funds managed by the ANR within the Investissements d'Avenir program under reference ANR-11-IDEX-0004-02. We thank F. Sennlaub for help with OIR experiments; J. Sahel and T. Debeir for helpful suggestions; Y. Zagar, M. Belle and C. Dominici for technical help; and K. Lyer for help with the initial phenotypic analysis. We also thank M. Tessier-Lavigne for the *Slit1*- and *Slit2*-knockout mice, J. Livet for the CAG:*Cre*^{ERTM} mouse line and R. Adams for the *Cdh5*:*Cre*^{ERT2} mouse line. VEGF-A–AP constructs were provided by C. Ruiz de Almodovar (Vesalius Research Center, Leuven, Belgium). pGEX-PAK-CRIB was a kind gift from M. Schwartz (Yale University, New Haven, Connecticut, USA). The *Slit2*(*lox*) mutant mouse line was established at the Mouse Clinical Institute (Institut Clinique de la Souris, Strasbourg, France) in the Targeted Mutagenesis and Transgenesis Department.

AUTHOR CONTRIBUTIONS

A.C. and A.E. supervised the project. A.C., A.E., N.R. and A.D. designed the experiments and wrote the manuscript. N.R., A.D., T.M., R.-A.N.C., G.G., B.C. and L.P.-F. performed the experiments and analyzed the data. L.M. generated the *Robo1*; *Robo2*^{lox} mice.

COMPETING FINANCIAL INTERESTS

The authors declare competing financial interests: details are available in the online version of the paper.

1. Ferrara, N. Vascular endothelial growth factor and age-related macular degeneration: from basic science to therapy. *Nat. Med.* **16**, 1107–1111 (2010).
2. Miller, J.W., Le Couter, J., Strauss, E.C. & Ferrara, N. Vascular endothelial growth factor a in intraocular vascular disease. *Ophthalmology* **120**, 106–114 (2013).
3. Lim, L.S., Mitchell, P., Seddon, J.M., Holz, F.G. & Wong, T.Y. Age-related macular degeneration. *Lancet* **379**, 1728–1738 (2012).
4. Brose, K. *et al.* Slit proteins bind Robo receptors and have an evolutionarily conserved role in repulsive axon guidance. *Cell* **96**, 795–806 (1999).
5. Kidd, T., Bland, K.S. & Goodman, C.S. Slit is the midline repellent for the robo receptor in *Drosophila*. *Cell* **96**, 785–794 (1999).
6. Ypsilanti, A.R., Zagar, Y. & Chedotal, A. Moving away from the midline: new developments for Slit and Robo. *Development* **137**, 1939–1952 (2010).
7. Koch, A.W. *et al.* Robo4 maintains vessel integrity and inhibits angiogenesis by interacting with UNC5B. *Dev. Cell* **20**, 33–46 (2011).
8. Zelina, P. *et al.* Signaling switch of the axon guidance receptor Robo3 during vertebrate evolution. *Neuron* **84**, 1258–1272 (2014).
9. Jones, C.A. *et al.* Robo4 stabilizes the vascular network by inhibiting pathologic angiogenesis and endothelial hyperpermeability. *Nat. Med.* **14**, 448–453 (2008).
10. Jones, C.A. *et al.* Slit2-Robo4 signalling promotes vascular stability by blocking Arf6 activity. *Nat. Cell Biol.* **11**, 1325–1331 (2009).
11. Huang, L. *et al.* Expression of Robo4 in the fibrovascular membranes from patients with proliferative diabetic retinopathy and its role in RF/6A and RPE cells. *Mol. Vis.* **15**, 1057–1069 (2009).
12. Zhou, W. *et al.* The role of SLIT-ROBO signaling in proliferative diabetic retinopathy and retinal pigment epithelial cells. *Mol. Vis.* **17**, 1526–1536 (2011).
13. Zhang, B. *et al.* Repulsive axon guidance molecule Slit3 is a novel angiogenic factor. *Blood* **114**, 4300–4309 (2009).
14. Yang, X.M. *et al.* Slit-Robo signaling mediates lymphangiogenesis and promotes tumor lymphatic metastasis. *Biochem. Biophys. Res. Commun.* **396**, 571–577 (2010).
15. Urbich, C. *et al.* HDAC5 is a repressor of angiogenesis and determines the angiogenic gene expression pattern of endothelial cells. *Blood* **113**, 5669–5679 (2009).
16. Kaur, S. *et al.* Robo4 signaling in endothelial cells implies attraction guidance mechanisms. *J. Biol. Chem.* **281**, 11347–11356 (2006).
17. Plump, A.S. *et al.* Slit1 and Slit2 cooperate to prevent premature midline crossing of retinal axons in the mouse visual system. *Neuron* **33**, 219–232 (2002).
18. Fouquet, C. *et al.* Robo1 and Robo2 control the development of the lateral olfactory tract. *J. Neurosci.* **27**, 3037–3045 (2007).
19. Morlot, C. *et al.* Structural insights into the Slit-Robo complex. *Proc. Natl. Acad. Sci. USA* **104**, 14923–14928 (2007).
20. Guo, C., Yang, W. & Lobe, C.G. A Cre recombinase transgene with mosaic, widespread tamoxifen-inducible action. *Genesis* **32**, 8–18 (2002).
21. Birdsey, G.M. *et al.* Transcription factor Erg regulates angiogenesis and endothelial apoptosis through VE-cadherin. *Blood* **111**, 3498–3506 (2008).
22. Guijarro-Muñoz, I. *et al.* The axonal repellent Slit2 inhibits pericyte migration: potential implications in angiogenesis. *Exp. Cell Res.* **318**, 371–378 (2012).
23. Sörensen, I., Adams, R.H. & Gossler, A. DLL1-mediated Notch activation regulates endothelial identity in mouse fetal arteries. *Blood* **113**, 5680–5688 (2009).
24. Yoshioka, K. *et al.* Endothelial PI3K-C2α, a class II PI3K, has an essential role in angiogenesis and vascular barrier function. *Nat. Med.* **18**, 1560–1569 (2012).
25. del Toro, R. *et al.* Identification and functional analysis of endothelial tip cell-enriched genes. *Blood* **116**, 4025–4033 (2010).
26. Wang, B. *et al.* Induction of tumor angiogenesis by Slit-Robo signaling and inhibition of cancer growth by blocking Robo activity. *Cancer Cell* **4**, 19–29 (2003).
27. Grieshammer, U. *et al.* SLIT2-mediated ROBO2 signaling restricts kidney induction to a single site. *Dev. Cell* **6**, 709–717 (2004).
28. Lu, W. *et al.* Disruption of ROBO2 is associated with urinary tract anomalies and confers risk of vesicoureteral reflux. *Am. J. Hum. Genet.* **80**, 616–632 (2007).
29. Long, H. *et al.* Conserved roles for Slit and Robo proteins in midline commissural axon guidance. *Neuron* **42**, 213–223 (2004).
30. Liu, D. *et al.* Neuronal chemorepellent Slit2 inhibits vascular smooth muscle cell migration by suppressing small GTPase Rac1 activation. *Circ. Res.* **98**, 480–489 (2006).
31. Wang, Y. *et al.* Norrin/Frizzled4 signaling in retinal vascular development and blood brain barrier plasticity. *Cell* **151**, 1332–1344 (2012).
32. Adams, R.H. & Eichmann, A. Axon guidance molecules in vascular patterning. *Cold Spring Harb. Perspect. Biol.* **2**, a001875 (2010).
33. Maisonpierre, P.C. *et al.* Angiopoietin-2, a natural antagonist for Tie2 that disrupts *in vivo* angiogenesis. *Science* **277**, 55–60 (1997).
34. Lu, X. *et al.* The netrin receptor UNC5B mediates guidance events controlling morphogenesis of the vascular system. *Nature* **432**, 179–186 (2004).
35. Ridgway, J. *et al.* Inhibition of Dll4 signalling inhibits tumour growth by deregulating angiogenesis. *Nature* **444**, 1083–1087 (2006).
36. Hellström, M. *et al.* Dll4 signalling through Notch1 regulates formation of tip cells during angiogenesis. *Nature* **445**, 776–780 (2007).
37. Larrivée, B. *et al.* ALK1 signaling inhibits angiogenesis by cooperating with the Notch pathway. *Dev. Cell* **22**, 489–500 (2012).
38. Small, E.M., Sutherland, L.B., Rajagopalan, K.N., Wang, S. & Olson, E.N. MicroRNA-218 regulates vascular patterning by modulation of Slit-Robo signaling. *Circ. Res.* **107**, 1336–1344 (2010).
39. Fish, J.E. *et al.* A Slit/miR-218/Robo regulatory loop is required during heart tube formation in zebrafish. *Development* **138**, 1409–1419 (2011).
40. Ridley, A.J. *et al.* Cell migration: integrating signals from front to back. *Science* **302**, 1704–1709 (2003).
41. Connor, K.M. *et al.* Quantification of oxygen-induced retinopathy in the mouse: a model of vessel loss, vessel regrowth and pathological angiogenesis. *Nat. Protoc.* **4**, 1565–1573 (2009).
42. Mehlen, P., Delloye-Bourgeois, C. & Chedotal, A. Novel roles for Slits and netrins: axon guidance cues as anticancer targets? *Nat. Rev. Cancer* **11**, 188–197 (2011).
43. Benedito, R. *et al.* Notch-dependent VEGFR3 upregulation allows angiogenesis without VEGF-VEGFR2 signalling. *Nature* **484**, 110–114 (2012).
44. Germain, S., Monnot, C., Muller, L. & Eichmann, A. Hypoxia-driven angiogenesis: role of tip cells and extracellular matrix scaffolding. *Curr. Opin. Hematol.* **17**, 245–251 (2010).

ONLINE METHODS

Mice. The *Slit2*–conditional knockout mouse line, in which exon 8 is flanked by *loxP* sites, was established at the Mouse Clinical Institute–Institut Clinique de la Souris (MCI/ICS, Illkirch, France; http://www-mci.u-strasbg.fr). This allele is predicted to produce a truncated Slit2 protein in which the final amino acid residue is F204, just after the end of the first leucine-rich domain (D1). This truncated protein is therefore unable to bind and activate Robo receptors. The targeting vector was constructed as follows: three fragments of 4.9, 0.4 and 3.5 kb (respectively, the 5′, floxed and 3′ arms) were amplified by PCR using 129S2/SvPas DNA as a template and sequentially subcloned in an MCI proprietary vector. This MCI vector has a floxed neomycin-resistance cassette. The linearized construct was electroporated into 129S2/SvPas mouse embryonic stem (ES) cells. After selection, targeted clones were identified by PCR using external primers and further confirmed by Southern blot with a 5′ external probe. Two positive ES cell clones were injected into C57BL/6J blastocysts, and the male chimeras derived gave germline transmission. The Neo cassette was excised by intercrossing with transgenic mice expressing Flp recombinase. All other knockout mouse lines (*Slit1* and *Slit2* (ref. 17), *Robo1* (ref. 29), *Robo2*^{lox} (ref. 28) and *Robo1*; *Robo2*^{lox} (ref. 45)) have been previously described and were validated. Floxed mice were crossed with *Cdh5*:*Cre*^{ERT2} (refs. 23,24) and CAG:*Cre*^{ERTM} mice[20]. We induced gene inactivation in pups at P0 with a single injection of tamoxifen (350 µg/g; Sigma, T5648) diluted in corn oil (Sigma, C8267). The *Rosa26*^{YFP} line (Jackson Laboratory) was used to monitor Cre expression (**Supplementary Fig. 2d**). Mice of a mixed genetic background and of either sex were used. The phenotypes of mutant mice were analyzed postnatally, between P3 and P17. In each experiment, tamoxifen-injected Cre-negative littermate pups were used as controls. Littermate pups of the same body weight were used in all cases. All animal procedures were performed in accordance with institutional guidelines (Université Pierre et Marie Curie, Comité Charles Darwin, Institut National de la Santé et de la Recherche Médicale, and Yale University).

Immunostaining. For whole-mount immunostaining, retinas were collected at P7. They were then fixed in 4% paraformaldehyde (PFA) in 0.12 M phosphate buffer for 15 min. Next, retinas were dissected in PBS and incubated in TNBT (10 mM Tris, pH 7.4, 150 mM NaCl, 0.5% blocking reagent (PerkinElmer, FP1012), 0.5% Triton X-100) for 2 h at room temperature. Retinas were incubated overnight at 4 °C in primary antibodies diluted in TNBT, after which retinas were washed with TNT (100 mM Tris, pH 7.4, 150 mM NaCl, 0.05% Triton X-100). Retinas were then incubated at room temperature for 2 h with secondary antibodies diluted in TNBT. Next, retinas were washed in TNT and incubated with 0.01 mg/ml IB4-FITC (Life Technologies, I21411) in PBLEC (1 mM PBS, 1 mM $MgCl_2$, 1 mM $CaCl_2$, 0.1 mM $MnCl_2$, 1% Triton X-100).

For immunostaining on sections, eyes were collected at P7 and fixed in 4% PFA for 1 h at room temperature. A hole was made in the cornea, and the eyes were incubated for 1 h in 10% sucrose (VWR, 27478.296) in 0.12 M phosphate buffer and then overnight at 4 °C in 30% sucrose in 0.12 M phosphate buffer. Eyes were then embedded and frozen in 0.12 M phosphate buffer containing 7.5% gelatin (Sigma, 62500) and 10% sucrose. 20-µm sections were cut with a cryostat (Leica, CM3050S). These sections were blocked in PBS containing 0.2% gelatin (VWR) and 0.25% Triton X-20 (PBS-GT) for 1 h and incubated overnight at room temperature with primary antibodies diluted in PBS-GT. Then the sections were incubated with secondary antibodies diluted in PBS-GT and 10 µg/ml Hoechst (Sigma, B2883).

The primary antibodies used were anti-Dll4, 2 µg/ml (R&D Systems, AF1389); anti-Vegfr2, 2 µg/ml (R&D Systems, AF644); anti–Neuropilin-1, 2 µg/ml (R&D Systems, AF566); anti-Collagen IV, 1/100 (Novotec, 20451); anti–Erg-1/2/3, 2 µg/ml (Santa Cruz, sc-353); anti-Calretinin, 2 µg/ml (Millipore, MAB1568); anti-Calbindin, 1 µg/ml (Swant, cb38-A); anti-PKCα, 1/500 (Sigma, P4334); and anti-GFP (Life Technologies, A11122; Abcam, ab13970). The secondary antibody used was Alexa 647–donkey anti-rabbit (Jackson ImmunoResearch, 711-605-152), Alexa 649–bovine anti-goat (Jackson ImmunoResearch, 805-495-180) or Cy3-donkey anti-rabbit (Jackson ImmunoResearch, 711.165.152).

We imaged the immunostained sections with an inverted confocal microscope (Olympus) or with a Nanozoomer 2.0 slide scanner (Hamamatsu).

***In situ* hybridization.** For *in toto* hybridization, we collected retinas after fixation as described above and dehydrated them with increasing concentrations of methanol (25%, 50%, 75% and 100%) in 0.1% PBS-Tween 20 (Sigma, P1379). For *in situ* hybridization on sections, we directly embedded and froze the eyes in Optimal Cutting Temperature compound without fixation. 20-µm sections were cut with a cryostat.

Antisense riboprobes were labeled with digoxigenin-11D-UTP (Roche) as described previously[46] by *in vitro* transcription of mouse cDNAs encoding *Slit1* (ref. 47), *Slit2* (ref. 48), *Slit3* (nucleotides 2,270–4,642) or *Plxnd1* (ref. 49). A mouse *Slit2* cDNA specific for exons 8–9 was amplified by PCR and cloned into pBluescript. Whole-mount retinas and retinal sections were hybridized as described previously[48].

In situ hybridization images were obtained with a DM6000 microscope (Leica) and CoolSNAP CCD camera (Roper).

Binding assay. Binding on flat-mounted retinas was performed as previously described[7] using VEGF-A–AP constructs (provided by C. Ruiz de Almodovar, Vesalius Research Center)[50] and Slit2-D2–AP, Slit1-D2–AP and Slit3-D2–AP fusion proteins[18].

Branch point quantification and vasculature analysis. Vessels were stained with 0.01 mg/ml IB4-FITC (Life Technologies, I21411). IB4-labeled retinas were imaged with a Nanozoomer slide scanner (Hamamatsu). Branch point numbers were quantified with Biologic CMM Analyser Software developed by N. Elie[51], and the retinal area was calculated with NDP-Viewer (Hamamatsu). Vascular density and vascular progression analysis were quantified with ImageJ. To measure retinal vascular density, we quantified the surface area of IB4 staining and of the total retina to obtain a ratio of coverage. To determine vascular progression, we measured the radius of the retina (*D*) and the distance from the optic nerve to the developing vascular front (*d*) and calculated the ratio *d*/*D*. At least 12 ratio (*d*/*D*) measurements were completed for each retina.

Proliferation analysis. We performed the proliferation analysis using the Click-iT EdU Alexa Fluor 488 Imaging Kit (Life Technologies, C10337). P3 or P7 pups were injected with 300 µg of EdU (5 mg/ml) and were killed 2 h later. We stained whole-mount retinas with anti–Erg-1/2/3 and IB4 biotin conjugate followed by Cy3-donkey anti-rabbit, 1/200 (Jackson ImmunoResearch, 711.165.152) and Alexa 647–conjugated streptavidin, 2 µg/µl (Jackson ImmunoResearch, 016-600-084). EdU staining was done according to the manufacturer's protocol. We imaged the retinas with a Nanozoomer slide scanner. EdU$^+$ and Erg-1/2/3$^+$ double-labeled nuclei were counted as proliferating endothelial cells. One 45° wedge was quantified for each retina. Double-labeled cells were counted in a 250-µm-wide region localized at the angiogenic front to calculate the percentage of proliferating endothelial cells.

The xCELLigence RTCA DP analyzer was used to measure the proliferation of control and *ROBO1*- and *ROBO2*-knockdown HUVECs in response to complete ECGM-2 medium (Lonza) or Slit2 (6 nM, R&D Systems). E-16 tissue culture plates (ACEA Biosciences) coated with 0.1% gelatin were seeded with 5,000 cells per well. The plates were monitored every 15 min for 48 h. For each condition, at least three replicate wells were analyzed.

Endothelial cell quantification. We stained P7 retinas with anti–Erg-1/2/3 and quantified the number of Erg-1/2/3–positive nuclei in one 45° wedge. We also quantified Erg-1/2/3–positive nuclei in retinal veins and in the retinal vascular plexus and determined the number of endothelial cells per millimeter of vein or per 50 µm of blood vessel.

Apoptosis analysis. P7 and P17 retinas were collected after fixation as described above. They were incubated for 2 h in 0.2% Triton X-100 PBS, washed three times with PBS and incubated for 10 min at room temperature in TdT buffer (30 mM Tris, 150 mM sodium cacodylate, 1 mM $CoCl_2$, pH 7.5) and then for 120 min at 37 °C with the TUNEL enzyme (Roche, 1767305001; 6 µl per milliliter of TdT buffer) and Biotin-16 dUTP (Roche; 6 µM) in TdT buffer. The retinas were incubated in TB buffer (300 mM NaCl, 30 mM sodium citrate), washed in PBS and blocked in 2% BSA in PBS. Next, we incubated the retinas with Cy3-coupled streptavidin (Jackson Laboratory, 016-160-084) 1/1,000 in

doi:10.1038/nm.3849

PBS and stained with Isolectin B4-FITC 0.01 mg/ml (Life Technologies, I21411). Retinal sections were incubated for 45 min in 0.2% Triton X-100 PBS and 1 h with TUNEL enzyme, Biotin-16 dUTP in TdT buffer.

We performed the *in vitro* apoptosis analysis using cleaved caspase-3 staining (Cell Signaling, 9661S) of confluent HUVEC monolayers. 24 h after siRNA transfection, the confluent cells were cultured for another 24 h with EBM2 or with EBM2 supplemented with 50 ng/ml VEGF-A, after which cleaved caspase-3 staining was performed.

Retraction analysis. We stained P7 retinas with anti–collagen-IV and Isolectin B4-FITC 0.01 mg/ml (Life Technologies, I21411) as described above and imaged them with a Nanozoomer slide scanner. The number of collagen IV^+ and $IB4^-$ vessels per field was counted. For each retina, we quantified three fields at the level of the angiogenic front and three in the remodeling plexus[43].

Adenoviral constructs. We generated a chimeric Robo1-Fc construct by using PCR to amplify the region of rat Robo1 encoding the first two immunoglobulin domains in the extracellular domain (amino acids 31–258) and then fusing this region to Fc by inserting it into pFUSE-hIgG1-Fc1 (InvivoGen) and then subcloning into pENTR1A (Invitrogen). Thereafter, the insert was transferred into pAd/CMV/V5/DEST using the Gateway System (Invitrogen). For *in vivo* experiments, we injected mouse pups intraperitoneally with 5×10^8 PFU in 50 µl at P12 and P13 and killed the mice at P17. We used at least six pups per group. No pups were excluded during this experiment. Control virus expressed eGFP (built from pEGFP-N1, Clontech).

Cell culture, treatment and cell-surface biotinylation. Human umbilical artery endothelial cells, HUVECs and human dermal microvascular endothelial cells were obtained from Lonza and cultured in ECGM-2 (Lonza). Human retinal microvascular endothelial cells were obtained from Cell Systems (ACBRI 181) and cultured in CSC Complete Medium (4Z0-500, Cell Systems). To assess the effects of Slit2 and of silencing of *ROBO1* and *ROBO2* on gene expression, we starved HUVECs overnight in EBM-2 supplemented with 0.1% FBS and treated them with Slit2 (6 nM) or VEGF-A (3 nM, R&D Systems) for 24 h. For stimulation with sDLL4, we precoated six-well plates with 10 µg/ml sDLL4 (R&D Systems) before plating cells, and we harvested the cells after 24 h. Uncoated plates served as a control. VEGFR2 surface biotinylation was done as described[52]. VEGFR2 internalization was measured as described[52]. Briefly, HUVECs were grown to confluence and starved overnight in EBM2 with 0.5% FBS. Cells were rinsed, incubated with EZ-Link Sulfo-NHS-SS-Biotin (0.25 mg/ml, Thermo Scientific) at 4 °C for 1 h in PBS and rinsed with 50 mM glycine in PBS to stop the reaction. A portion of the cells were harvested and used to determine total biotinylated cell surface protein. The remaining cells were rinsed once with cold media + 1% BSA, stimulated with EBM2 containing Slit2 at 37 °C for different times and then rinsed and incubated twice for 20 min each time on ice with the membrane-nonpermeable reducing agent GSH (45 mM, Sigma) in 75 mM NaCl, 75 mM NaOH, 1 mM EDTA, 1% BSA. GSH was quenched by incubating twice for 5 min each time with iodoacetamide (5 mg/ml) in PBS. Cell lysates were prepared using NP-40 lysis buffer (Roche). 200 µg of lysate was immunoprecipitated with 50 µl of NeutrAvidin beads (Invitrogen) at 4 °C overnight, after which the beads were rinsed and resuspended in Laemmli SDS sample buffer. Samples were analyzed by SDS–PAGE followed by western blotting with anti-VEGFR2 (Cell Signaling Technology, 9698).

siRNA transfection. siRNAs (FlexiTube siRNA) were purchased from Qiagen. We transfected HUVECs with 25 pmol siRNA per six-well plate with 2.5 ml RNAiMax (Invitrogen) according to the manufacturer's instructions. Cells were used for experiments 48 h after transfection.

***In vitro* sprouting assay.** 24 h after siRNA transfection, we resuspended HUVECs (250,000 cells per well in six-well plates) in fibrinogen solution (2.5 mg/ml fibrinogen (Sigma) in EBM-2 (Lonza) supplemented with 2% FBS and 50 mg/ml aprotinin (Sigma)) and plated the mixture on top of a precoated fibrin layer (fibrinogen solution clotted with 1 U thrombin (Sigma-Aldrich) for 20 min at 37 °C). The second layer of fibrin was clotted for 1 h at 37 °C. Wi-38 cells (250,000 cells per well; Lonza) in EBM-2 supplemented with 2% FBS and 25 ng/ml VEGF were then plated on top of the fibrin layers. Cultures were incubated at 37 °C, 5% CO_2. After 4–6 d, cultures were labeled with 4 mg/ml Calcein AM (Sigma) for 1 h and imaged by fluorescence using a standard FITC filter.

Scratch assay. We grew confluent monolayers of HUVECs in six-well plates. 24 h after siRNA transfection, we starved the cells for 18 h in EBM-2 medium with 1% FBS. We created a horizontal wound in the confluent monolayer using a sterile 200-µl pipette tip. Next, we incubated the cells in EBM-2 supplemented with VEGF-A (25 ng/ml) or Slit2 (1 µg/ml) at 37 °C for 16 h. Pictures of scratch wounds were taken just before stimulation (time 0) and after 16 h. We calculated the extent of cell migration using ImageJ software.

RAC1 activation assay. Our assay used the RAC Interactive Binding (CRIB) region of the RAC effector protein PAK1 (PAK1-CRIB) fused to GST to pull down activated, GTP-bound RAC1. We induced Top10 *E. coli* cells (Invitrogen) harboring pGEX-PAK-CRIB (a kind gift from M. Schwartz, Yale University) with isopropyl β-D-1-thiogalactopyranoside (0.3 mM). After 3 to 4 h at 37 °C, the cells were centrifuged at 2,800*g* for 5 min and lysed in 20 mM Tris-HCl at pH 7.2, 150 mM NaCl, 1% Triton X-100, 10 mM $MgCl_2$, 1 mM PMSF, lysozyme (1 µg ml^{-1}), DTT (10 mM), 10 µg DNase I and protease inhibitors (Sigma). We purified the PAK-GST fusion proteins from the bacterial lysate with glutathione-Sepharose 4B beads (GE Healthcare Life Sciences) and then washed the beads with binding/wash buffer (50 mM Tris-Cl at pH 7.2, 150 mM NaCl, 10 mM DTT, 1% Triton X-100 and protease inhibitors). Next, we incubated the PAK-GST beads with HUVEC lysate (NP-40 lysis buffer; Roche) for 45 min at 4 °C, washed the beads in binding/wash buffer (50 mM Tris-Cl at pH 7.2, 150 mM NaCl, 10 mM $MgCl_2$, 1% Triton X-100 and protease inhibitors), and resuspended in 2× Laemmli sample buffer. RAC1 was detected by western blotting using antibodies to RAC1 (1/1,000, Cell Signaling, 2465).

Quantitative real-time PCR analysis. We isolated RNA using the RNeasy Plus Kit (Qiagen). Next, 1 µg RNA was retrotranscribed with the iScript cDNA Synthesis kit (Bio-Rad). We performed real-time qPCR reactions in duplicate using the CFX-96 Real Time PCR system (Bio-Rad). Quantitative PCR primers were obtained from Qiagen. GAPDH and actin or housekeeping genes encoding GAPDH, actin and CD31 were used as controls for experiments using HUVECs or mouse lung endothelial cells, respectively. We calculated fold changes using the comparative C_T method. We used one of the three experimental control samples as a reference.

Western blots. We dissected retinas and froze them in liquid nitrogen. Next, they were lysed for 1 h at 4 °C in 50 mM HEPES, 150 mM NaCl, EDTA, 5 mM NP40 1%, and protease inhibitor cocktail (Roche, 1187358001). The samples were boiled for 5 min with Laemmli loading buffer.

For experiments with lung endothelial cells and HUVECs, we lysed the cells in RIPA buffer (20 mM Tris, pH 7.5, 60 mM NaCl, 1% Triton X-100, 0.5% deoxycholic acid, 0.1% sodium dodecyl sulfate, 10% glycerol, 25 mM β-glycerol phosphate, 50 mM sodium fluoride, 2 mM sodium pyrophosphate, 1 mM sodium orthovanadate, and 1× protease inhibitor cocktail (Calbiochem)).

We separated the proteins using SDS–PAGE (Bio-Rad, 456-1086) and transferred them to a nitrocellulose membrane (Bio-Rad). Membranes were blocked in TBS, 0.1% Tween-20, 5% non-fat dry milk and then incubated at 4 °C overnight with primary antibodies diluted in blocking buffer (1 µg/ml). Membranes were washed and incubated with peroxidase-conjugated secondary antibodies (1:2,000; Pierce) in blocking buffer for 1 h at room temperature. We visualized bands with ECL Prime (Amersham) or with enhanced-chemoluminescence western blotting detection reagents (Pierce). We imaged membranes using the GE Healthcare ImageQuant LAS-4000 imaging system or the Fusion FX7 chemiluminescence system (Fisher).

Antibodies. We used anti-ROBO1 (R&D Systems, MAB7118; Abcam, ab7279), anti-Robo2 (Abcam, ab75014 for mouse and ab64158 for human), anti-ROBO4 (MAB2454, R&D Systems), anti-RAC1 (Cell Signaling, 2465S), anti-pPAK1(Ser144)/PAK2(Ser141) (Cell Signaling, 2606), anti-PAK (Cell Signaling, 2604), p44/42 MAPK (p-ERK, Cell Signaling, 9106), anti-p44/42 MAPK (total ERK, Cell Signaling, 9102), anti-pAKT(Ser)473 (Cell Signaling, 4060), anti-AKT (Cell Signaling, 4691) and anti-actin (1:1,000, Sigma, A5060).

Lung endothelial cell isolation. We harvested mouse lungs at P21, minced them and incubated them in 5 mL Dulbecco's modified Eagle's medium containing 2 mg/mL collagenase I (Invitrogen) for 45 min at 37 °C with shaking every 15 min followed by filtering through a 40-µm nylon mesh (BD Falcon). The cells were then centrifuged at 1,000*g* for 5 min at 4 °C, resuspended in buffer 1 (0.1% bovine serum albumin, 2 mM EDTA, pH 7.4, in PBS), and incubated with anti-rat immunoglobulin G–coated magnetic beads (Invitrogen) precoupled with rat anti-mouse platelet/endothelial cell adhesion molecule-1 (PECAM-1; MEC13.3, BD Pharmingen, 553370) for 30 min at 4 °C in an overhead shaker. Beads were separated from the solution with a magnetic particle concentrator (Dynal MPC-S, Invitrogen). The beads were washed five times with buffer 1 and centrifuged for 5 min at 1,000*g*, and the supernatant was removed. The purified endothelial cells were then cultured in ECGM-2 (Promocell). For western blot analysis, lung endothelial cells (2×10^5) were seeded in 60-mm dishes and cultured for 24 h in ECGM-2 at 37 °C and 5% CO_2.

Oxygen-induced retinopathy model. OIR was induced as described in ref. 41. P7 pups, together with their mother, were placed in 75% O_2 until P12 (Biospherix). At P12, the pups were removed, placed in a normal atmosphere, injected with 350 µg/g of tamoxifen and placed with a nursing mother. Eyes were collected at P17, and the retinas were stained with IB4 as described above. The avascular area was quantified as described in ref. 42.

Data quantification and statistics. All data quantification was done by an observer blinded to the experimental conditions. For the *in vivo* experiments, the quantification and the genotyping were done by two different investigators. We quantified at least three different litters per condition. We did not perform randomization into groups. For all strains, phenotypic analysis was done on littermates of similar body weight (2.4 g ± 0.4 g (s.d.) at P7 and 6.1 g ± 1.4 g (s.d.) at P17; average weights from three different litters). Statistical analyses of the mean and variance were performed with Prism 6 (GraphPad Software). We performed a two-tailed Student's *t*-test when the number of retinas was equal to or greater than 10; otherwise, we performed a two-tailed Mann–Whitney test.

45. Domyan, E.T. *et al.* Roundabout receptors are critical for foregut separation from the body wall. *Dev. Cell* **24**, 52–63 (2013).
46. Marillat, V. *et al.* Spatiotemporal expression patterns of slit and robo genes in the rat brain. *J. Comp. Neurol.* **442**, 130–155 (2002).
47. Nguyen-Ba-Charvet, K.T. *et al.* Multiple roles for slits in the control of cell migration in the rostral migratory stream. *J. Neurosci.* **24**, 1497–1506 (2004).
48. Di Meglio, T. Nguyen-Ba-Charvet, K.T., Tessier-Lavigne, M., Sotelo, C. & Chédotal, A. Molecular mechanisms controlling midline crossing by precerebellar neurons. *J. Neurosci.* **28**, 6285–6294 (2008).
49. Chauvet, S. *et al.* Gating of Sema3E/PlexinD1 signaling by neuropilin-1 switches axonal repulsion to attraction during brain development. *Neuron* **56**, 807–822 (2007).
50. Xu, Y. *et al.* Neuropilin-2 mediates VEGF-C-induced lymphatic sprouting together with VEGFR3. *J. Cell Biol.* **188**, 115–130 (2010).
51. Jones, E.A., Yuan, L., Breant, C., Watts, R.J. & Eichmann, A. Separating genetic and hemodynamic defects in neuropilin 1 knockout embryos. *Development* **135**, 2479–2488 (2008).
52. Lanahan, A. *et al.* The neuropilin 1 cytoplasmic domain is required for VEGF-A-dependent arteriogenesis. *Dev. Cell* **25**, 156–168 (2013).

doi:10.1038/nm.3849